Sensing atmospheric turbulence by GNSS phase observations

M. Vennebusch, S. Schön, *Institut für Erdmessung, Leibniz Universität Hannover*
Email: vennebusch@ife.uni-hannover.de

BIOGRAPHIES

Markus Vennebusch received his diploma in Geodesy from the University of Bonn, Germany in 2002. Then he worked in the VLBI research group at the Institute of Geodesy and Geoinformation at the University of Bonn and finished his PhD thesis in 2007. After one year at GeoForschungsZentrum Potsdam he started his research work on atmospheric turbulence at the Institut für Erdmessung at Leibniz Universität Hannover.

Steffen Schön is professor for positioning and navigation at the IfE since 2006. Since 2003, he has been involved in several GPS projects at DGFI Munich (Germany) and IGMS TUGraz (Austria), especially on landslide monitoring, development of GPS quality indicators, and studies on turbulence theory. His current research interests are the correction and assessment of systematic errors in GNSS, like e.g., absolute antenna calibration, receiver clock modeling, and improved stochastic model of GNSS observations.

ABSTRACT

Turbulent motions within the atmospheric boundary layer generate high-frequency variations of the water vapor content of the air and thus of the refractivity index field. Since electromagnetic waves are sensitive to such variations, atmospheric turbulence consequently causes phase fluctuations which can also be sensed by GNSS signals. In addition, parameters derived from GNSS signals such as estimated tropospheric signal delays can be used to analyse effects of atmospheric turbulence.

In the following we provide some background of atmospheric turbulence theory and we describe a simulation method to generate variations of slant tropospheric delays. The temporal stochastic behaviour of these simulated delays is expressed in terms of temporal structure functions and is compared with their theoretically expected behaviour. As an example we present time series of simulated slant tropospheric delay variations for a realistic GPS observation scenario.

INTRODUCTION/ ATMOSPHERIC TURBULENCE

Signals of Global Navigation Satellite Systems (GNSS), as well as all other electromagnetic waves are effected by atmospheric attenuation, scintillation, and delay (Spilker 1996). Especially the dry (hydrostatic) and wet (non-hydrostatic) signal delays are one of the main error sources which have to be adequately accounted for when using GNSS signals for e.g. precise surveying or timing purposes. These tropospheric delays show both long periodic and short periodic variations in the range from months to hours as well as from minutes to seconds (and even less). The short periodic behaviour is caused by high-frequency variations of the refractivity index n which are generated by turbulent air motions within the first approximately 2000 [m] of the atmosphere (i.e., the atmospheric boundary layer).

These refractivity variations yield random phase fluctuations which should be accounted for within the stochastic model of the GNSS data analysis. In addition, these phase fluctuations can be used to study the turbulent medium the signal has passed.

In order to provide a mathematical description of the random refractivity variations the refractivity index $n(\boldsymbol{x}, t)$ at a location $\boldsymbol{x}$ and at time t is separated into $n = n_0 + \Delta n$, with a steady state component n_0 and a highly variable Δn whose variations are considered to be generated by a complex superimposition of swirls (called 'eddies') that interact nonlinearly to create random, chaotic motions. Due to this random behaviour no deterministic description has been found yet (Wallace and Hobbs 2006). The net effect, however, can be described statistically via the energy spectrum, which relates the amount of total turbulence kinetic energy to the different scales of turbulence elements ('eddies'). Various authors derived analytical models for the most important parts of this spectrum (inertial subrange). In the following, the von Karman spectrum is used (Wheelon 2001):

$$\Phi_n(\kappa) = \frac{0.033\, C_n^2}{(\kappa^2 + \kappa_0^2)^{\frac{11}{6}}} \propto \kappa^{\frac{-11}{3}},\ 0 < \kappa < \kappa_S. \qquad (1)$$

Here, C_n^2 is the so-called refractivity structure constant, $\kappa = 2\pi/l$ indicates the wavenumber corresponding to eddy

size l, κ_0 and κ_s are the wavenumbers corresponding to the inner and outer scale lengths l_0 and L_0, respectively. More details about atmospheric turbulence and wave propagation in turbulent media can be found in e.g. Stull (1988) and Wheelon (2001).

In the following we show how high-frequency variations of tropospheric delays can be simulated using parameters of atmospheric turbulence and we assess the stochastic properties of those simulated slant delay time series. These simulations form the basis for the assessment of turbulence effects observed in tropospheric delays derived from real GNSS data. Another motivation for the analysis of tropospheric delay variations derived from high-frequency GNSS data is due to the increasing observation rates (1 to 100 [Hz]), which are -for example- required for navigation purposes or earthquake monitoring. At these data rates the correlating effects of the tropospheric fluctuations can no longer be omitted.

TEMPORAL STOCHASTIC BEHAVIOUR OF TROPOSPHERIC DELAYS

The von Karman spectrum (Eq. 1) follows a so-called power-law behaviour with an exponent $\alpha = -11/3$ (Agnew 1992). This shows that atmospheric turbulence is characterised as a non-stationary stochastic process which should thus not be expressed in terms of (auto-)correlation functions or power spectral densities (Kasdin 1995). A more appropriate tool to assess the temporal behaviour of a non-stationary process X is the temporal structure function (Wheelon 2001)

$$D_X(\tau) = \langle [X(t+\tau) - X(t)]^2 \rangle, \tag{2}$$

with $\langle \cdot \rangle$ denoting an ensemble average and τ indicating the time lag between two values of X. The temporal differencing removes data trends and thus generates a difference process which is usually stationary even if the original time series is not stationary.

A typical example of a temporal structure function loglog-plot is shown in Fig. 1. The loglog-plot allows an easy association of the slope of the structure function to the power-law exponent and thus allows an easy identification of the relevant stochastic process. Theoretically, for small time lags τ of several seconds (region A) structure function values should be close to zero. In practice, however, for those time lags the curve often starts with a zero slope and thus indicates the presence of white noise. For medium ranges (region B) the dominant noise type of the process can be assessed by the slope of the structure function. For turbulence processes, this region typically shows slopes of 2/3 to 5/3. For larger time lags τ (region C) the structure function approaches an asymptotic value (also referred to as *sill*) of $2 \cdot \sigma_X$, i.e., twice the variance of X. For these time lags with zero slope, the data is considered as being uncorrelated (so-called saturation region). In geostatistical terminology (Olea 1999), the structure function is commonly called (semi-)variogram with the time lag τ, at which the

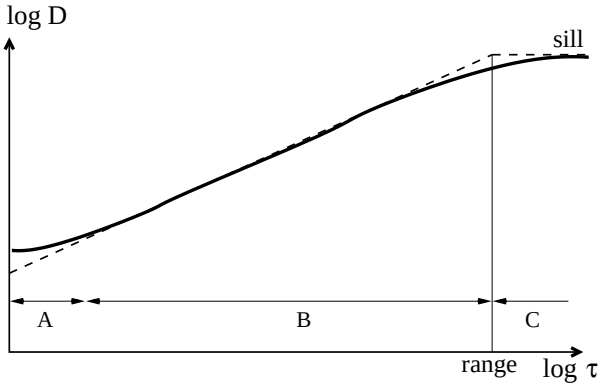

Figure 1: Example for temporal structure function behaviour.

structure function reaches the constant value (sill), referred to as *range*.

An explicit expression for the temporal structure function of phase measurements is provided by (Wheelon 2001) as follows:

$$D_\varphi(\tau) = D_T(\tau) = 1.564 R k^2 C_n^2 k_0^{-\frac{5}{3}} \times \left(1 - \frac{2^{\frac{1}{6}}}{\Gamma\left(\frac{5}{6}\right)} (\kappa_0 v \tau)^{\frac{5}{6}} K_{\frac{5}{6}}(\kappa_0 v \tau)\right), \tag{3}$$

with R denoting the length of the propagation path, k being the respective wavenumber of the microwave signal, κ_0 being the wavenumber corresponding to the outer scale length and v being the wind speed. The unit of this explicit structure function is [rad], thus dividing by k^2 again yields the structure function in a metric unit. Since we consider only tropospheric fluctuations, Eq. (3) is equivalent to the structure function of tropospheric delays. However, for real data, $D_\varphi(\tau)$ also contains contributions from additional stochastic processes, such as e.g., residuals receiver clock errors or multipath effects.

Figure 2 shows the explicit temporal structure function, Eq. (3), for various typical turbulence parameter sets evaluated for a fixed observation geometry with an elevation of 13.5 [°].

Curve 1 represents a structure function for average turbulence conditions (with average fluctuations/sill of $\approx 1.2 \cdot 10^{-6}$ [m^2] and a range of $\approx$ 200 [s]) and serves as a reference set which the other curves are compared with. Reducing the integration height H by a factor of 1/2 (i.e., to 1000 [m], curve 2) also reduces the fluctuations/sill by the same factor to $\approx 0.6 \cdot 10^{-6}$ [m^2] and slightly reduces the range to approximately 180 [s].

Increasing the wind speed v from 8 [m/s] to 15 [m/s] (curve 3) does not affect the sill but significantly reduces the range (and thus the correlation length) by approximately 100 [s]. In other words: Increasing wind speed acts decorrelating on both phase fluctuations and tropospheric delays (details will be given below).

Increasing the outer scale length L_0 from 3000 [m] to 6000 [m] (curve 4) increases both the average fluctuations

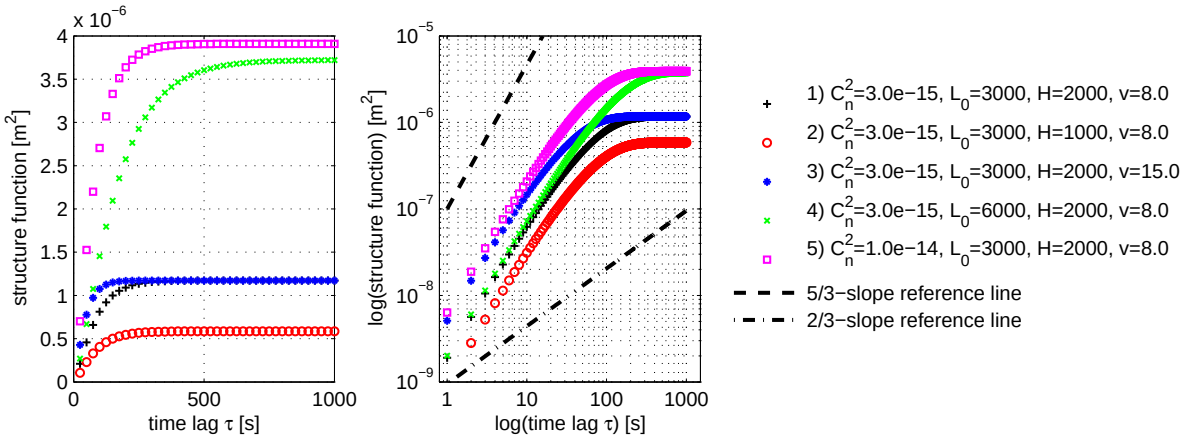

Figure 2: Explicit temporal structure functions of slant tropospheric delays for typical conditions of atmospheric turbulence for a fixed observation geometry with an elevation of 13.5 [°] (left: linear axes, right: logarithmic axes).

(i.e., the sill) to $\approx 3.7 \cdot 10^{-6}$ [m^2] and the range to ≈ 300 [s].

Finally, increasing the refractivity structure constant to $C_n^2 = 1.0 \cdot 10^{-14}$ [m$^{-2/3}$] (i.e., by a factor of 3.3, curve 5) linearly scales the fluctuations/sill by the same factor. Compared to the average parameter set (curve 1), the range has not been changed.

In addition, for all parameter combinations considered, the explicit temporal structure functions show a clear 5/3 power-law behaviour for the first ≈ 80 [s] (see loglog-plot on the right hand side of Fig. 2). Depending on the specified turbulence parameters (especially the outer scale length L_0) a continous decrease of the exponent can be seen. At a maximum of approximately 500 [s] the exponent reaches zero (for these examples).

In the following we will demonstrate a simulation procedure for tropospheric delay variations and we will assess the stochastic properties of the generated time series in terms of their temporal structure functions.

COVARIANCE EXPRESSION OF SLANT TROPOSPHERIC DELAYS

Common procedures for the simulation of time series with a predefined stochastic behaviour are based on Cholesky decompositions or eigenvalue decompositions of variance-covariance matrices whose elements define the scatter and the covariances (and thus the correlations) between the values to be simulated (e.g. Johnson and Wyatt 1994, Searle 1982).

Variances and covariances of tropospheric delays can be derived by integrating the spectrum of refractivity variations along the lines-of-sight (Wheelon 2001). A general covariance expression for tropospheric delays has been derived by Schön and Brunner (2008). Based on the von Karman spectrum and the assumptions of height-independent C_n^2, local isotropy, uniform wind speed and wind direction this formulation describes the covariance of two tropospheric slant delays $T_A^i(t_A)$ and $T_B^j(t_B)$ at two stations A and B, to two satellites i and j and at two epochs t_A and t_B. In its most general formulation the co-variance expression reads:

$$\langle T_A^i(t_A), T_B^j(t_B) \rangle =$$

$$\frac{12}{5} \frac{0.033}{\Gamma\left(\frac{5}{6}\right)} \frac{\sqrt{\pi^3} \kappa_0^{-\frac{2}{3}} 2^{-\frac{1}{3}}}{\sin \varepsilon_A^i \sin \varepsilon_B^j} C_n^2 \times \tag{4}$$

$$\int_0^H \int_0^H (\kappa_0 d)^{\frac{1}{3}} K_{-\frac{1}{3}}(\kappa_0 d)\, dz_1\, dz_2,$$

where Γ denotes the gamma function and K the modified Bessel function of second kind. In order to analyse the impact of wind speed and wind direction on explicit temporal structure functions and on simulated slant delay variations, special attention will be paid to the parameter d which is the length of the vector $\boldsymbol{d} = \boldsymbol{r}_2 + \boldsymbol{\rho} - \boldsymbol{v}\Delta t - \boldsymbol{r}_1$ between the actual integration points. This vector is a function of the line-of-sight vectors $\boldsymbol{r}_1$ and $\boldsymbol{r}_2$, the baseline vector $\boldsymbol{\rho}$, the wind vector $\boldsymbol{v}$ and the time difference Δt between two tropospheric delays. The value of $\boldsymbol{d}$ determines the value of the integration kernel and thus the covariance between two tropospheric delays as well as its temporal variation. The temporal evolution of $\boldsymbol{v}\Delta t$ is the most variable contribution to $\boldsymbol{d}$.

In the following we try to illustrate the variation of $\boldsymbol{d}$ for the basic case of one station and one satellite. Consequently, $\boldsymbol{\rho} = \boldsymbol{0}$ and $\boldsymbol{r}_2$ and $\boldsymbol{r}_1$ are the unit vectors pointing to the same satellite at different epochs t_i and t_j, respectively. The contributions to the vector $\boldsymbol{d}$ can be separated into (i) a *geometric part* resulting from the varying directions of the lines-of-sight with time, and (ii) the *atmospheric part*.

For the temporal separation $\Delta t = t_i - t_1$ between the first observation and an observation at epoch t_i, the distance between the first white circle and the i-th white circle represents the geometric contribution to the separation distance (at a given height) which is due to the satellite movement on its orbit. For any temporal variation $\Delta t = t_k - t_m$ the

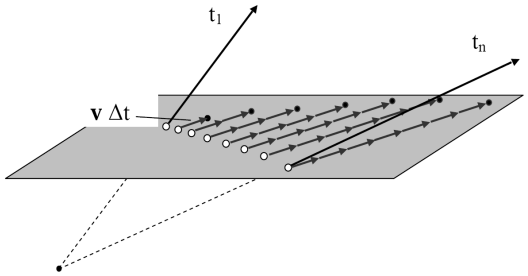

Figure 3: Visualisation of geometric and atmospheric contributions to the separation distance d.

corresponding geometric contribution can be represented by the distance between the k-th and the m-th white circle.

In addition, the atmospheric contribution is considered and superimposed onto the geometric one. This contribution stems from the assumption of 'frozen turbulence' (Taylor's hypothesis), i.e., that a volume of atmospheric turbulence structures travels with a constant velocity over the sensor. These contributions are parameterised by the product of the wind vector and the temporal separation $\boldsymbol{\Delta} = \boldsymbol{v}\Delta t$. In Fig. 3 these contributions for a unique time interval Δt are represented by the black arrows. The vector addition leads to the black circles, which indicate the virtual intersection points which should be used for the computation of the separation distance.

Depending on the wind direction, the superposition of both contributions can increase or reduce the values of the separation distance compared to that one obtained from the geometric contributions only. In case of Fig. 3 an additive superposition is obtained.

A rough estimate of the possible magnitudes of the different contributions (geometric contribution including station separation and the atmospheric contribution) shows that even for moderate wind velocities of some [m/s], the atmospheric contribution quickly dominates the total separation distance. Consequently the wind velocity -in combination with the wind direction- governs the correlation and decorrelation process. For more details, the reader is referred to Schön and Brunner (2007) and Schön and Brunner (2008).

ANALYSIS OF SIMULATED TROPOSPHERIC DELAY VARIATIONS

Using real or simulated observation geometries as well as adequate turbulence parameters a fully occupied variance-covariance matrix $\boldsymbol{\Sigma}_T$ of tropospheric delays T can be set up to generate simulated tropospheric delay variations. In the following, these variations will be simulated by using an orthonormal matrix $\boldsymbol{G}$ containing the eigenvectors of $\boldsymbol{\Sigma}_T$, a diagonal matrix $\sqrt{\boldsymbol{\Lambda}}$ containing the square roots of the eigenvalues of $\boldsymbol{\Sigma}_T$ on its main diagonal, and a vector $\boldsymbol{x}$ of gaussian random numbers with zero mean and unit variance via (Searle 1982):

$$\boldsymbol{y} = \boldsymbol{G}\sqrt{\boldsymbol{\Lambda}}\boldsymbol{x}. \tag{5}$$

Note that for the following simulations, each different set of five realisations has been generated using the same set of Gaussian vectors $\boldsymbol{x}$ (see Eq. (5)).

For the simulation of slant tropospheric delay variations a realistic geometry of a rising GPS satellite is used (see also Vennebusch and Schön 2009). During an observation period of 1000 [s] ($\approx$ 17 [min]) the satellite rises from 10 [°] to 17 [°] elevation at an azimuth of 201 [°]. Using a sampling rate of 0.1 [Hz] the entire observation period thus yields 100 observations. Figures 4 and 5 show variance-covariance matrices obtained by numerically integrating Eq. (4) for various sets of turbulence parameters. Parameter set 1 discribes an average turbulence condition with refractivity structure constant $C_n^2 = 0.3 \times 10^{-14}$ [$\mathrm{m}^{-2/3}$], outer scale length $L_0 = 3000$ [m], wind speed $v = 8$ [m/s], integration height $H = 2000$ [m] and wind direction (azimuth) $\alpha_v = 0$ [°]. This parameter set serves as a reference for comparisions of the impact of variations in the turbulence parameters on (co-)variances, correlations, slant tropospheric delay variations, and their temporal structure functions.

- Parameter set 1: For this parameter set the variances vary between $0.75{\cdot}10^{-6}$ [m^2] for the lowest elevations (10 [°]) and $0.48 \cdot 10^{-6}$ [m^2] for the highest elevations (17 [°]). Due to the changing geometry both the variance-covariance matrix and the correlation matrix do not have a clear band structure. This property is also reflected by the moderate variations in the respective anti-diagonal plots. For example, after 10 epochs an average correlation of 0.44 with an average scatter of 0.04 is visible. After 20 epochs the average correlation coefficient is 0.13 with a scatter of 0.04.

  The simulated slant tropospheric delay variations vary in the range of ± 2 [mm] with an average variance of $4.6{\cdot}10^{-7}$ [m^2]. All temporal structure functions show a clear 5/3 power-law behaviour for the first $180 - 200$ [s]. One temporal structure function (of this and of the other parameter sets) shows a negative slope for time lags larger than 200 [s]. This is caused by the characteristics of the respective random vector $\boldsymbol{x}$ used for the simulations.

- Parameter set 2: Changing the wind azimuth α_v from 0 [°] to 90 [°] has a significant decorrelating effect on the simulated tropospheric delays. Compared to parameter set 1, the variances remain unchanged while the covariances decrease much faster and show smaller variations. This is also reflected in reduced correlation lengths of 0.11 after 10 epochs (100 [s]) and 0.01 after 20 epochs (200 [s]) (both with a negligible scatter).

  Compared to the first parameter set, the simulated slant tropospheric delay peak-to-peak variations hardly changed but the entire time series show a much rougher behaviour which obviously agrees with the reduced correlation lengths. The average variance is $\approx 6 \cdot 10^{-7}$ [m^2], which is also reflected in the larger values of the temporal structure functions. The slopes of the temporal structure functions, however,

are generally smaller than 5/3, especially for small time lags τ. This behaviour results from the increased roughness (reduced correlation) of the simulated time series yielding an apparent high-frequency noise contribution.

- Parameter set 3: Increasing the wind speed v from 8 [m/s] to 15 [m/s] also has a decorrelating effect on tropospheric delay variations. This can again be observed in variances which are similar to those of the previous parameter set and by quickly decreasing covariances leading to average correlation values of 0.15 after 10 epochs and 0.01 after 20 epochs (and approximately the same correlation scatter as for parameter set 1).

  The simulation procedure generates tropospheric delay variations with increased average variance (of $\approx 6.5 \cdot 10^{-7}$ [m^2]) and consequently larger temporal structure function values. Again, compared to parameter set 1, no exact 5/3 power-law behaviour can be observed for small time lags τ.

- Parameter set 4: The impact of changing the outer scale length L_0 from 3000 [m] to 6000 [m] can be observed in larger variances (of $\approx 2.3 \cdot 10^{-6}$ [m^2] at low elevations to $\approx 1.3 \cdot 10^{-6}$ [m^2] at higher elevation) and longer correlation lengths. After 10 epochs the average correlation is still 0.7 and 0.38 after 20 epochs with scatter variations of 0.02 after 10 epochs and 0.04 after 20 epochs.

  Due to the larger (co-)variances the peak-to-peak variations of the simulated tropospheric delay variations increased to approximately ± 3 [mm] with a rather smooth entire behaviour. This also leads to temporal structure functions with a clear 5/3 power-law behaviour.

COMPARISONS AND DISCUSSION

Three of the temporal structure functions of simulated tropospheric delays (Fig. 4 and 5) can be compared to the explicit temporal structure functions shown in Fig. 2:

- The temporal structure function of tropospheric delays simulated with average turbulence parameters (section 1 in Fig. 4) shows the same 5/3 power-law behaviour and approximately the same fluctuations/sill of $1.2 \cdot 10^{-6}$ [m^2] and a similar range of ≈ 200 [s] as the first curve in Fig. 2. However, for small time lags τ the values of the explicit temporal structure function are approximately four times larger than the corresponding values of the structure function of simulated slant delays.

- Comparing the structure function of section 3 (Fig. 5, using a wind speed of 15 [m/s]) with the structure function of section 1 and with the third explicit temporal structure function shows that the structure function of simulated tropospheric delays behaves as predicted: The average fluctuations/sill remains almost unchanged and structure function values for small time lags τ are larger when using higher wind speed. The same holds for the range, i.e., for a larger wind speed the range (and thus the correlation lengths) decrease. But, as for section 1, explicit temporal structure function values for small time lags τ are about three times larger than those of simulated slant delays (curve 3).

- Finally, a comparison of the structure function of section 4 (Fig. 5, for increased outer scale length) with the one of section 1 (Fig. 4) shows that for small time lags values the corresponding structure functions almost perfectly agree. In addition, for larger outer scale lengths and for larger time lags larger variations/sills are observed. This is the same behaviour as observed in the corresponding explicit temporal structure functions. But again, for small time lags the explicit temporal structure function values are approximately four times larger than those of the simulated slant delays.

In summary, the general behaviour (e.g., the 5/3 slope and the variations due to parameter changes) of the structure functions of simulated tropospheric delays agrees with the general behaviour of the explicit temporal structure functions. However, especially for small time lags τ discrepancies of a factor of almost five are observed. This needs to be further investigated.

SUMMARY & OUTLOOK

In this paper we investigated the simulation of tropospheric slant delays based on turbulence theory. Using different values for turbulence parameters (such as the refractivity structure constant C_n^2, the outer scale length L_0, the integration height H and the wind speed v) the generated non-stationary time-series change accordingly. In our example scenario, a decorrelation (i.e., a noisier time series) is obtained by increasing the wind speed v and/or the outer scale length L_0.

The stochastic behaviour of these time series are best assessed by temporal structure functions which showed the expected behaviour, i.e., a 5/3 power-law behaviour and similar responses to parameter changes as those observed in the theoretical expressions of the temporal structure functions.

In future, these results will be compared to the time series and structure functions of slant delays estimated from real GNSS phase measurements. Current activities concentrate on both the estimation of high-resolution (i.e., 1 [Hz]) zenith tropospheric delays using Precise Point Positioning (PPP) approaches, and on the analysis of double-differenced phase observations from specially designed GNSS networks for the investigation of atmospheric turbulence.

1.) Reference set (average turbulence conditions)

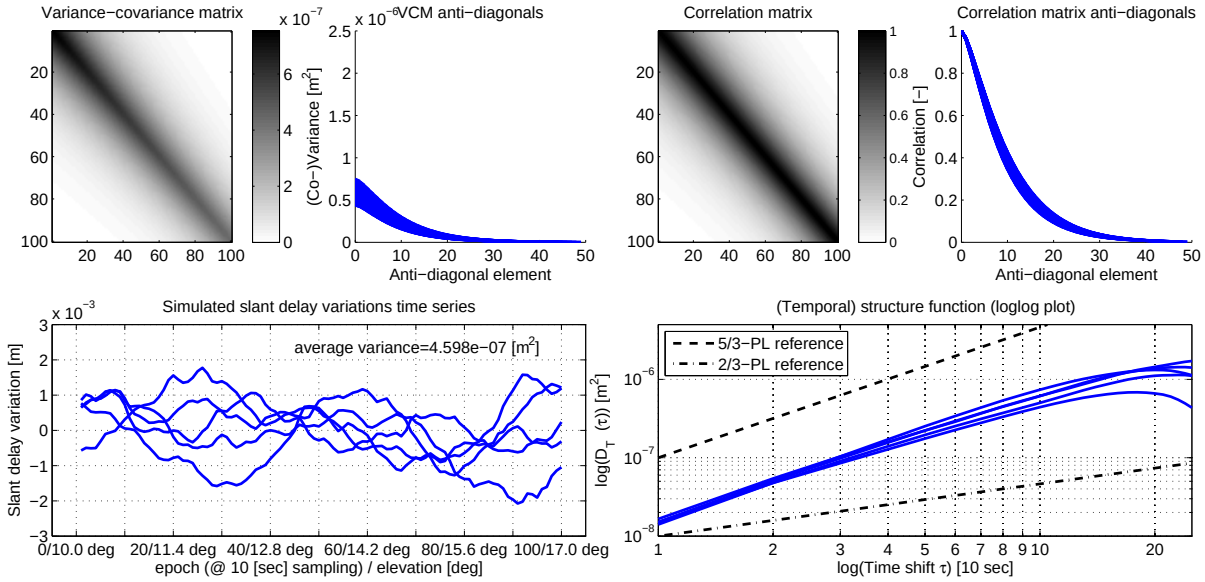

2.) wind azimuth increased

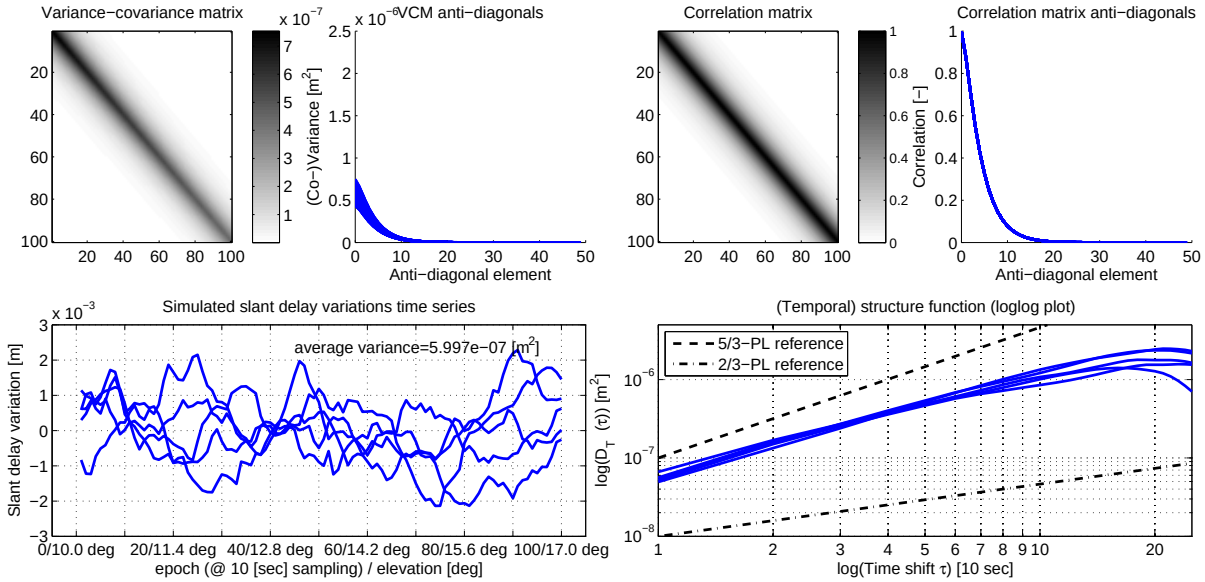

Figure 4: Variance-covariance matrices, correlation matrices, anti-diagonal plots, simulated slant tropospheric delay variations and their temporal structure functions. Section 1.) Average turbulence parameters ($C_n^2 = 0.3 \times 10^{-14}$ [$\mathrm{m}^{-2/3}$], outer scale length $L_0 = 3000$ [m], integration height $H = 2000$ [m], wind speed $v = 8$ [m/s] and wind direction (azimuth) $\alpha_v = 0$ [°]), section 2.) same as 1.), but wind azimuth increased to 90 [°].

3.) wind speed increased

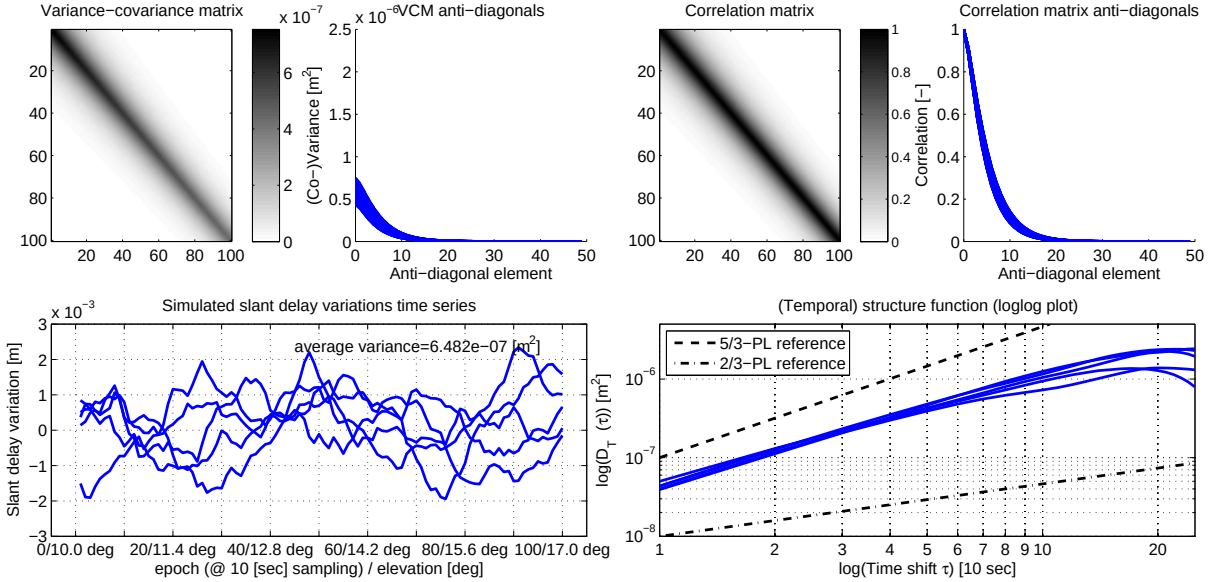

4.) outer scale length increased

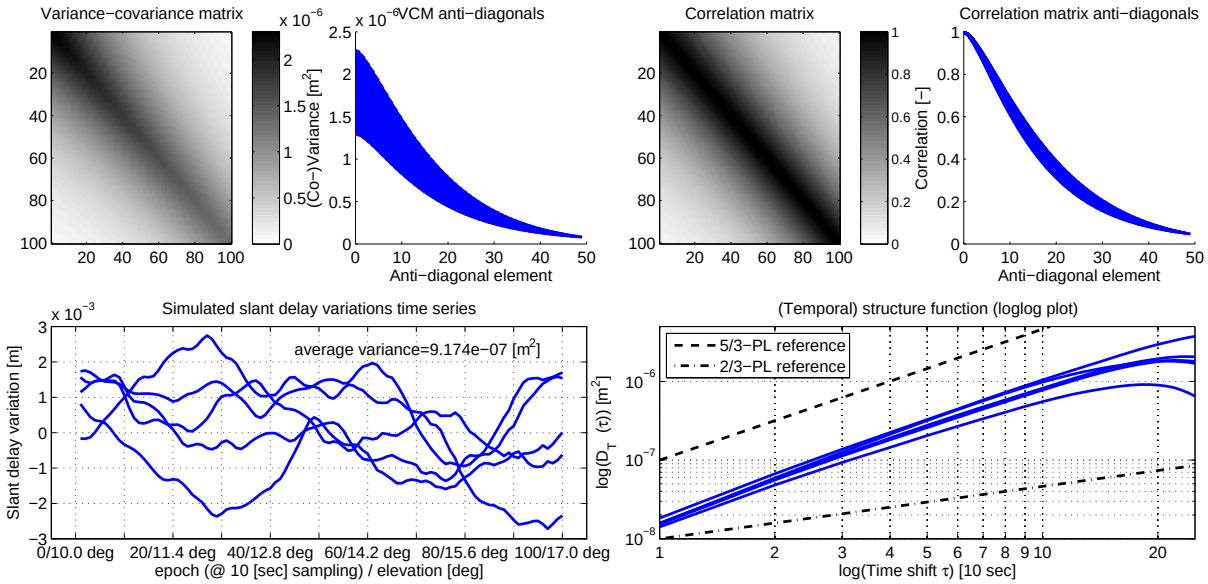

Figure 5: Variance-covariance matrices, correlation matrices, anti-diagonal plots, simulated slant tropospheric delay variations and their temporal structure functions. Section 3.) same as 1.), but wind speed increased to 15 [m/s], section 4.) same as 1.), but outer scale length L_0 increased to 6000 [m].

ACKNOWLEDGEMENTS

The authors thank the German Research Foundation (Deutsche Forschungsgemeinschaft) for its financial support (SCHO 1314/1-1).

REFERENCES

Agnew DC: The time-domain behaviour of power-law noises, GRL 19(4), 333-336, 1992.

Johnson HO, Wyatt FK: Geodetic network design for fault-mechanics studies, manu geod 19:309-323, 1994.

Kasdin NJ: Discrete Simulation of Colored Noise and Stochastic Processes and $1/f^{\alpha}$ Power Law Noise Generation, Proceedings of the IEEE, Vol. 83, No. 5, 1995.

Olea RA: Geostatistics for engineers and earth scientists, Kluwer Academic Publishers, Boston, 1999.

Schön S, Brunner FK: Treatment of refractivity fluctuations by fully populated variance-covariance matrices. Proc. 1st Colloquium Scientific and Fundamental Aspects of the Galileo Programme, Toulouse, 2007.

Schön S, Brunner FK: Atmospheric turbulence theory applied to GPS carrier-phase data, J geod 82(1): 47-57, 2008.

Searle SR: Matrix Algebra Useful for Statistics, Wiley, 1982.

Spilker JJ: Tropospheric effects on GPS, in: Parkinson BW and JJ Spilker (eds) Global Positioning System: theory and applications. Progress in Astronautics and Aeronautics. Vol. 163, AIAA, Washington D.C., 1996.

Stull RB: An Introduction to Boundary Layer Meteorology, Springer, 1988.

Vennebusch M, Schön S: Generation of slant tropospheric time series based on turbulence theory, submitted to Proceedings of 2009 IAG Scientific Assembly, 2009.

Wallace JM, Hobbs PV: Atmospheric science: an introductory survey, Elsevier, 2006.

Wheelon AD: Electromagnetic scintillation-I. Geometrical optics, Cambridge University Press, Cambridge, 2001.